Available online at www.sciencedirect.com
SCIENCE DIRECT®
Journal of volcanology and geothermal research
ELSEVIER
Journal of Volcanology and Geothermal Research 128 (2003) 65–88
www.elsevier.com/locate/jvolgeores

The 1998–1999 seismic series at Deception Island volcano, Antarctica

J.M. Ibáñez [a,b,*], E. Carmona [a], J. Almendros [a], G. Saccorotti [c], E. Del Pezzo [c], M. Abril [a], R. Ortiz [d]

[a] *Instituto Andaluz de Geofísica, Universidad de Granada, Campus de Cartuja s/n, 18071 Granada, Spain*
[b] *Departamento de Física Teórica y del Cosmos, Universidad de Granada, Granada, Spain*
[c] *Osservatorio Vesuviano, Istituto Nazionale di Geofísica e Vulcanología, Napels, Italy*
[d] *Departamento de Volcanología, Museo Nacional de Ciencias Naturales–CSIC, Madrid, Spain*

Received 15 May 2002; accepted 10 June 2003

Abstract

During the 1998–1999 Antarctic summer the pattern of seismic activity at Deception Island volcano changed significantly. The change was characterized by the occurrence of an intense swarm of volcano–tectonic (VT) earthquakes. More than 2000 VT earthquakes with S–P times smaller than 4 s were recorded in the period January–February 1999. Pure volcanic events were also detected; especially long-period (LP) events, volcanic tremor and some hybrid events. Seismic monitoring was performed using two short-period small-aperture arrays, among other instruments. Based on their signal-to-noise ratios we selected 863 VT earthquakes, 350 LP events and tremor episodes, and 9 hybrid events for analysis. We estimated apparent slowness and back-azimuth for all events using the Zero Lag Cross-Correlation array technique. Combining this information with S–P times and other indirect evidence, we identified two different source regions. LP seismicity is located less than 1–1.5 km southwest of the Fumarole array site. These events are likely to have a hydrothermal origin. VT earthquakes and hybrid events are located at depths of 0.3–10 km in an area under the bay of Deception Island. The area extends from the Fumarole array to the northeast with epicentral distances that range from 0.5 to 12 km. Most hypocenters are clustered in a small volume of around 8 km^3. The sources of the LP seismicity and the VT earthquakes are spatially distinct, which indicates that they are not produced by the same mechanisms. Moment magnitude analyses of the VT earthquakes provide an average magnitude of 0.5 and very low average stress drop, around 1 bar. A study of first motion of the P-waves suggests that the events in this small source region should have a variety of source mechanisms. This is supported by the existence of families of events with the same waveforms. The occurrence of repeating fracture processes with low stress drop and small fault dimensions can be explained by the lubrication of pre-existing zones of weakness by pressurized fluids. The most probable hypothesis that explains the generation of this seismic series at Deception Island is: a seismic series caused by the stress generated by the uplift of the source area due to a magmatic injection in depth. We favor this hypothesis since it is compatible with the majority of the characteristics of the seismicity and explains the spatial and temporal behavior of the series.

* Corresponding author. Tel.: +34-958248910; Fax: +34-958160907. *E-mail address:* ibanez@iag.ugr.es (J.M. Ibáñez).

0377-0273/03/$ – see front matter © 2003 Elsevier B.V. All rights reserved.
doi:10.1016/S0377-0273(03)00247-6

Keywords: volcanic seismicity; long-period events; volcano-tectonic earthquakes; magma injection; Antarctica

1. Introduction

The seismic activity associated with a volcanic environment is diverse and complex. Several types of seismic signals, with different signatures and frequency content, can be generated within a single volcanic region, and these characteristics are usually not the same for different volcanoes. Recently, however, we have realized that the physics underlying the generation of seismic energy in a volcano is not complex, and relatively simple mechanisms can be invoked to explain the different types of volcano seismicity. Following Chouet (1996), we can distinguish two main classes of source processes in active volcanic areas. The first one consists of the brittle fracture of the medium in response to stress, a purely elastic mechanism that generates the so-called volcano–tectonic (VT) earthquakes. In general, the spectral content of this type of signal is broadband with frequencies up to 50 Hz. The procedure for modelling tectonic earthquakes is well established. With the proper tools, the source parameters for such events can be calculated quickly and accurately. The second class of events requires the presence and movement of fluids with exchange elastic energy with the medium. Most of the theoretical models in use today were developed in the 1980s and 1990s by several authors, for example Crosson and Bame (1985), Chouet (1988, 1992), Dahm (1992), Julian (1994), Nakano et al. (1998), Hellweg (2000) and Neuberg et al. (2000). These models describe the physics of seismic sources when a large amount of fluid is present. In general, these theories describe the source of the seismic radiation as resulting from the trapping of acoustic waves due to the impedance contrast between magmatic/hydrothermal fluids and solid rock. The resulting waveforms and spectra may vary greatly, depending on the shape of the resonating cavity, excitation mechanism, and fluid properties (Kumagai and Chouet, 2000). In any case, they can be described as narrow-band events in contrast to the VT earthquakes, usually with very emergent first motions. We will refer to these signals generated with direct involvement of volcanic fluids generically as pure volcanic signals or long-period (LP) seismicity. They include event types as distinct as volcanic tremor, spasmodic tremor, harmonic tremor, LP events, tornillo events, gas-piston events, and more. In the present work we will distinguish only between LP events and tremor, by means of their short and long durations, respectively. Finally, a third, mixed mechanism sometimes occurs when brittle failure and fluid-driven resonance appear simultaneously in the recordings. This type of seismic signal is called as hybrid and is composed of a VT earthquake followed by a LP signal (Lahr et al., 1994).

The distribution of volcanic seismicity in space and time depends on the type of event and the level of volcanic activity. VT earthquakes have been recorded before, during, and/or after eruptions, but they may occur without eruptions (Benoit and McNutt, 1996) and eruptions may occur without VT earthquakes. Their hypocenters and even the source mechanisms are routinely determined using seismic networks. They are supposed to coincide with the volcanic conduit where magma is moving, and several studies map volcanic conduits using hypocenter locations of VT earthquakes (Klein et al., 1987; Lahr et al., 1994, etc). Pure volcanic signals are more difficult to locate; nevertheless they are more adequate to map the volcanic conduits, since they are generated only in presence of moving fluids (Almendros et al., 2002). Due to the emergent character of the pure volcanic events and their low-frequency content, classical (routine) seismic techniques are almost useless for solving the problem of source location. The study of volcanic seismicity requires the use of new instruments and configurations, in particular dense seismic arrays of seismometers. The analysis may be more complex and time-consuming, but we are able to obtain information about the locations of sources of volcanic signals, properties of the wavefield, and the shallow velocity structure under the array. LP seismicity is usually located at shallow depths (Lahr et al., 1994; Gil Cruz and Chouet, 1997; Ibáñez et al., 2000)

but deep LP events and tremor have been observed as well (Koyanagi et al., 1987). LP seismicity may appear just before eruptions or be associated with hydrothermal activity. Pure volcanic signals have been recorded at most volcanoes. Their significance as precursors to eruptive activity (Chouet, 1996) has been demonstrated by many examples: the 1991 eruption of Mount Pinatubo, Philippines (e.g. Ramos et al., 1999), Mount St. Helens, USA (e.g. Fehler, 1983), Galeras, Colombia (e.g. Narváez et al., 1997), Mount Redoubt, Alaska, USA (e.g. Chouet et al., 1994), and Kilauea, Hawaii, USA (e.g. Ohminato et al., 1998).

In the present work we analyze data recorded at Deception Island volcano, Antarctica, during the 1998–1999 summer field survey. Starting in January 1999, the seismic activity increased suddenly. Before the end of the season we recorded about 1500 VT earthquakes, and a similar number of purely volcanic events. Understanding this seismicity is important because the most recent eruptions at Deception Island was preceded by intense seismic swarms, similar to the series analyzed in this work. We start by classifying the recorded events and studying the temporal evolution of each event type. We use array techniques to estimate back-azimuths and apparent slownesses, and measure the S–P delay to determine hypocenter locations. The temporal and spatial distribution of the hypocenters and the appearance of several different mechanisms in a small source volume will lead us to a hypothesis about the cause of the seismic activity and its implications for the dynamics of the volcano.

2. Instruments and data

2.1. Seismic instruments

During the 1998–1999 Antarctic summer field survey at Deception Island we deployed a Guralp CMG40T broadband sensor, two short-period continuous recording stations, and two seismic arrays. One of the continuous recording stations, with a three-component sensor, was placed near the Spanish base, and the other, with a vertical component sensor, was used as a portable station and deployed in different places around the island.

The first array had an aperture of 320 m and was deployed near Obsidians Hill. It consisted of 13 vertical-component, short-period stations configured as two concentric semicircles with radii of 160 and 80 m, and a three-component sensor at the hub. However, Saccorotti et al. (2001) have documented slowness anomalies in the data recorded at the Obsidians array. Since we are not able to correct for these anomalies we will not use the data from this array. The second array had an aperture of 240 m and was deployed on the southern shore of Fumarole Bay, close to the most active fumarole system on the island. This array had seven vertical-component and three three-component stations, configured in two semicircles with radii of 120 and 60 m (Fig. 1). The seismometers of the external and internal semicircles were spaced at intervals of 45° and 60°, respectively. All instruments were Mark L4C sensors with flat response to 1 Hz. Both arrays were situated on alluvial fans. Each array was equipped with two eight-channel data acquisition systems (DAS). In Saccorotti et al. (2001) there is a complete description of the DAS. The antennas were operative between December 7, 1998, and February 25, 1999, when the Spanish base 'Gabriel de Castilla' closed operations for the season. Due to the high level of seismicity at the end of the field experiment, a permanent seismic station, with a vertical component sensor, was left near the Spanish base at the end of the survey. It operated for two more months. This station recorded at a low sampling rate (25 sps) in order to conserve storage space in the computer.

2.2. Characteristics of the seismicity

All seismic records were inspected visually and classified by their shapes and S–P times as: regional or VT earthquakes, LP events, hybrid events, or volcanic tremor. Regional events are not considered in this study, since they have no relationship to the volcanic activity. Spectra and spectrograms were computed for selected events

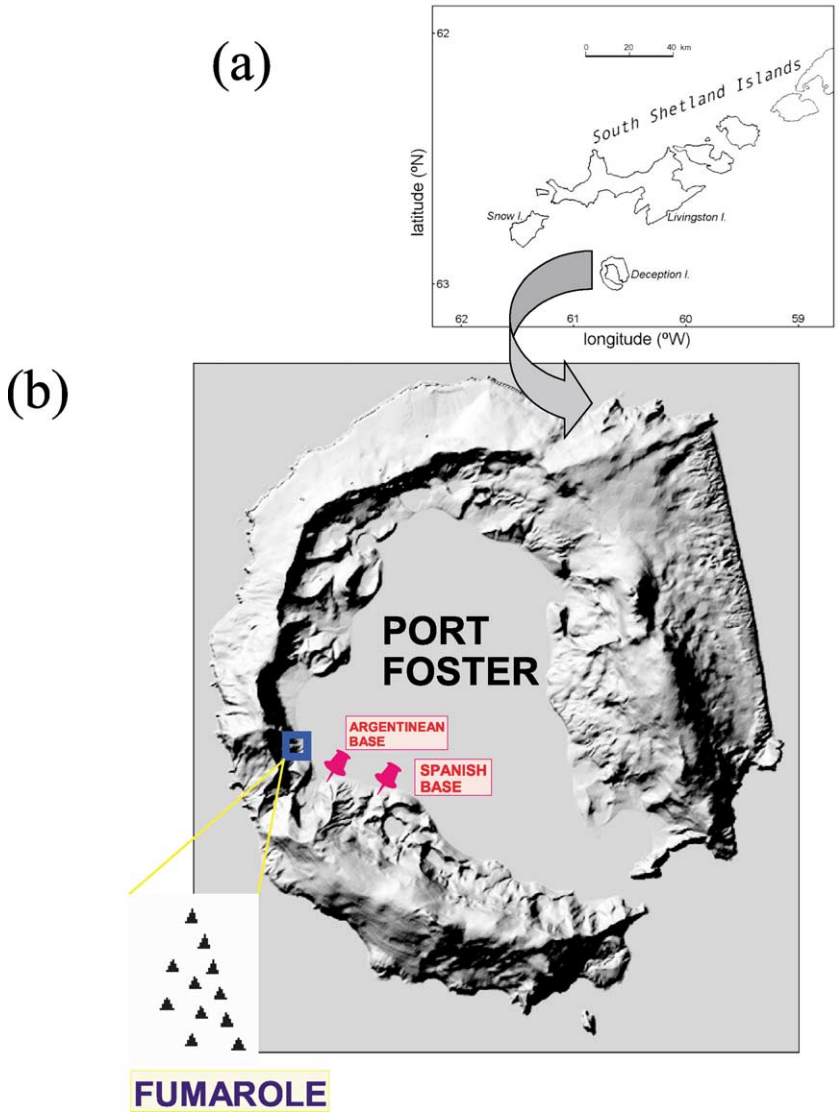

Fig. 1. (a) Map of the South Shetland Islands region, Antarctica, showing the position of Deception Island. (b) Map of Deception Island, showing the location and configuration of the seismic antenna used for the present analysis.

to determine the spectral content of each type of event.

2.2.1. VT earthquakes

Earthquakes with an S–P time less than 4 s are considered to be VT earthquakes. They have a clear P-wave arrival, usually impulsive, and the S-waves are easily identified on the horizontal components (Fig. 2). Their spectra show a very broad spectral content, with energy up to 40 Hz. In the particle motion we clearly see the arrivals of the P-waves and S-waves. Moreover, in the first S-wave onset we detect a sudden change in the horizontal motion. The change from linear to elliptical polarization is related to a delay between the arrivals of the E–W and the N–S components. This may be caused by S-wave splitting, which will be the topic of a future study.

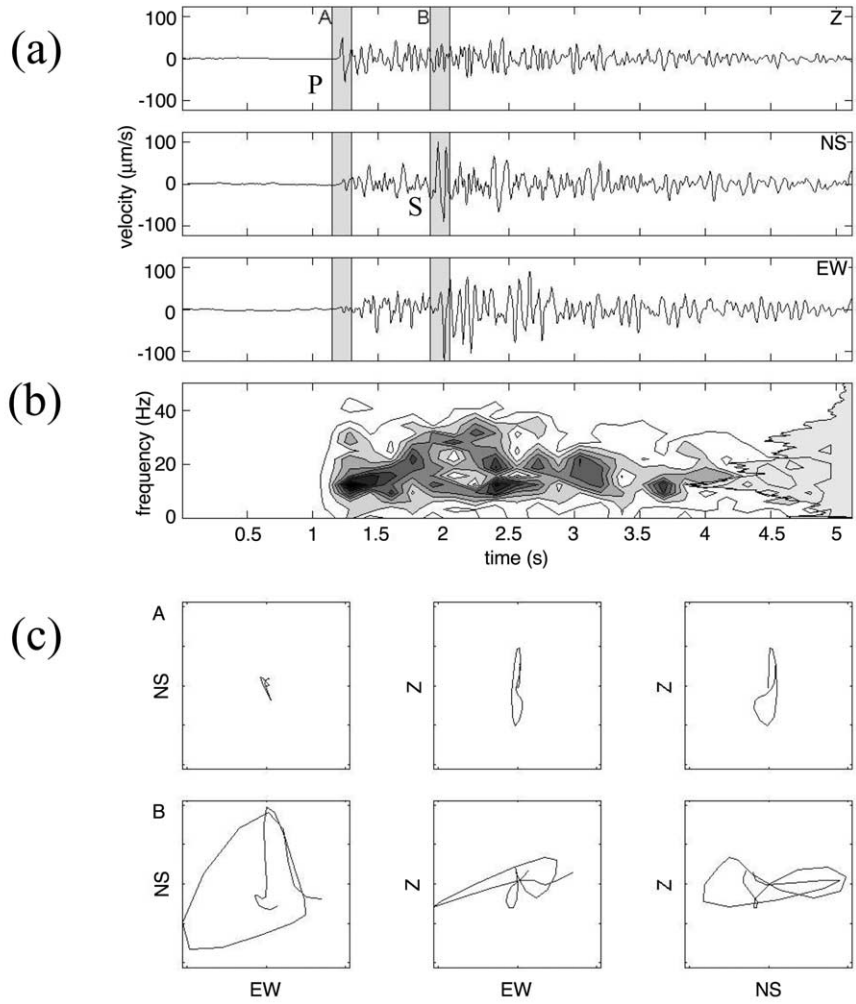

Fig. 2. Example of a VT earthquake recorded at Fumarole array. (a) Seismograms of the three components of the ground motion. The gray areas labelled A and B correspond to the arrival of the P-waves and S-waves, respectively. P and S represent the onset of the P-waves and S-waves over the seismogram, respectively. (b) Spectrogram of the vertical-component seismogram shown in (a). Superimposed at the right edge of the plot is the spectrum of the whole trace. (c) Particle motion diagram corresponding to the windows A and B in (a).

2.2.2. *LP events*

LP events at Deception Island have spindle-shaped envelopes and durations of a few tens of seconds (Fig. 3). In spectra and spectrograms, these signals are quasi-monochromatic, centered at frequencies between 1 and 6 Hz. The particle motions show that the first onsets might be composed of P-waves. However, suddenly they change to more complex patterns which can be interpreted as mixtures of surface waves (Ibáñez et al., 2000).

2.2.3. *Hybrid events*

These events begin with a high-frequency phase followed by a monochromatic signal similar to a LP event (Fig. 4). Spectral analysis reveals the different properties of these two distinct phases. The initial high-frequency portion has a broad spectrum, extending up to frequencies of 40 Hz. In contrast, the LP segment is quasi-monochromatic and peaks at low frequencies, around 1–6 Hz.

It is important to point out that some LP

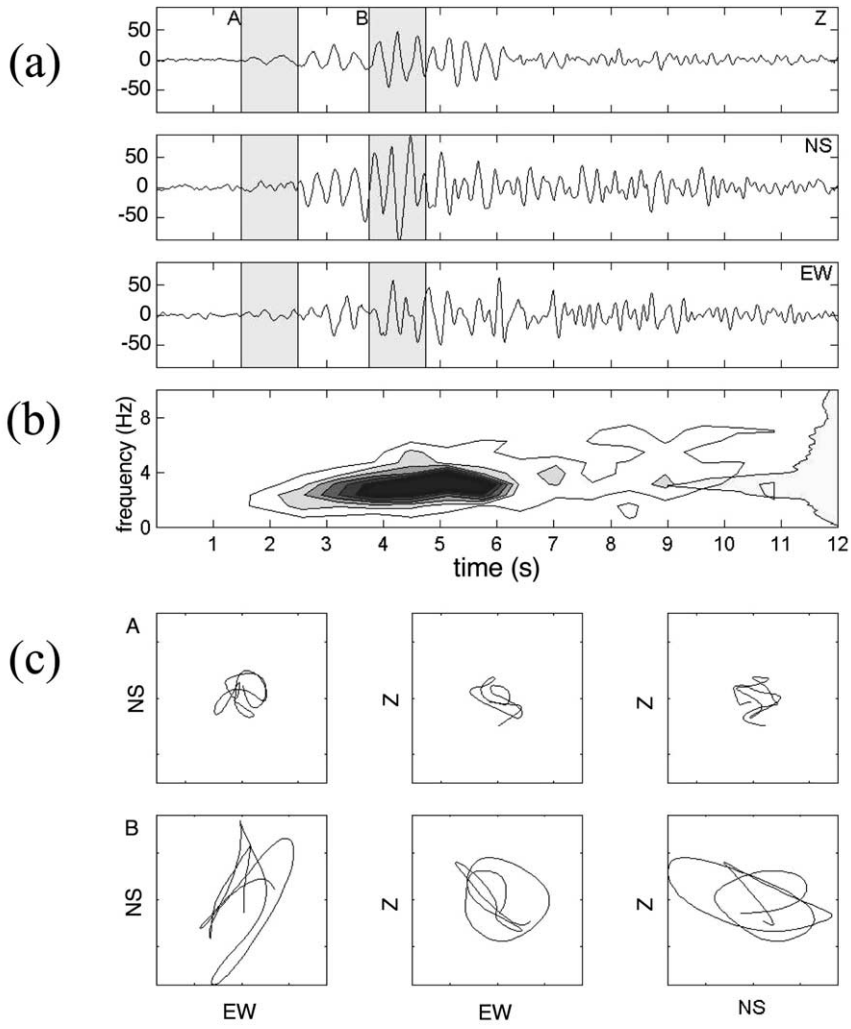

Fig. 3. Example of a LP event recorded at Fumarole array. (a) Seismograms of the three components of the ground motion. The gray areas labelled A and B correspond to the first arrival and the center of the low-frequency wave train, respectively. (b) Spectrogram of the vertical-component seismogram shown in (a). On the right side of the plot we show the spectrum of the whole trace. (c) Particle motion diagrams corresponding to windows A and B in (a).

events have low-energy, high-frequency initial phases, and thus might be confused with hybrid events. The difference is in the source mechanism of these high-frequency waves. For example, Ibáñez et al. (2000) initially used the term *hybrids* for a type of LP events with a strong high-frequency initial phase, due to their spectral properties. However, the definition of Lahr et al. (1994) states that the high-frequency component of a true hybrid is produced by a shear source. This condition is difficult to determine without proper instrumental coverage. In the case of Deception Island, we will confirm the hybrid nature of our signals by their proximity to the hypocenters of VT earthquakes.

2.2.4. *Volcanic tremor*

The presence of volcanic tremor at Deception Island volcano is well known since the first recording of its seismicity in the 1950s. The characteristics of tremor are similar to those observed for the LP events: a narrow spectral peak between

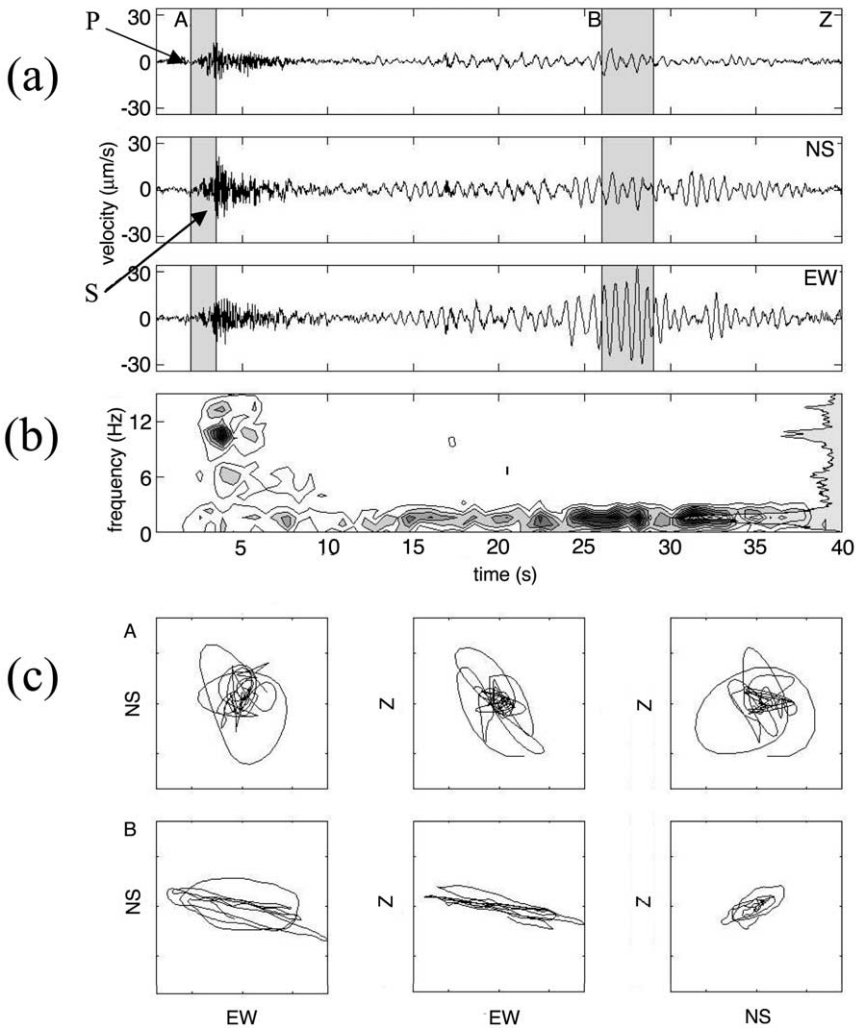

Fig. 4. Example of a hybrid event recorded at Fumarole array. (a) Seismograms of the three components of the ground motion. The gray areas labelled A and B correspond to the first high-frequency arrival and the center of the low-frequency wave train, respectively. P and S represent the onset of the P-waves and S-waves over the seismogram, respectively. (b) Spectrogram of the vertical-component seismogram shown in (a). On the right side of the plot is the spectrum of the whole trace. (c) Particle motion diagram corresponding to the windows A and B in (a).

1 and 3 Hz, and complex particle motion (Fig. 5). The main difference is the long duration of the tremor episodes. They may last for intervals from a few minutes to several days or weeks.

2.3. The evolution of the seismicity in time

The pattern of occurrence is different for the various event types. We counted the daily number of LP events recorded by the Fumarole array and the number of VT events recorded by the array and by the continuous recording station deployed near the Spanish base, in operation until the beginning of April 1999 (Fig. 6).

LP seismicity appears in swarms which last a few days and alternate with rest periods of several days. A total of 1800 LP events were recorded, with peak activity reaching about 150 events per

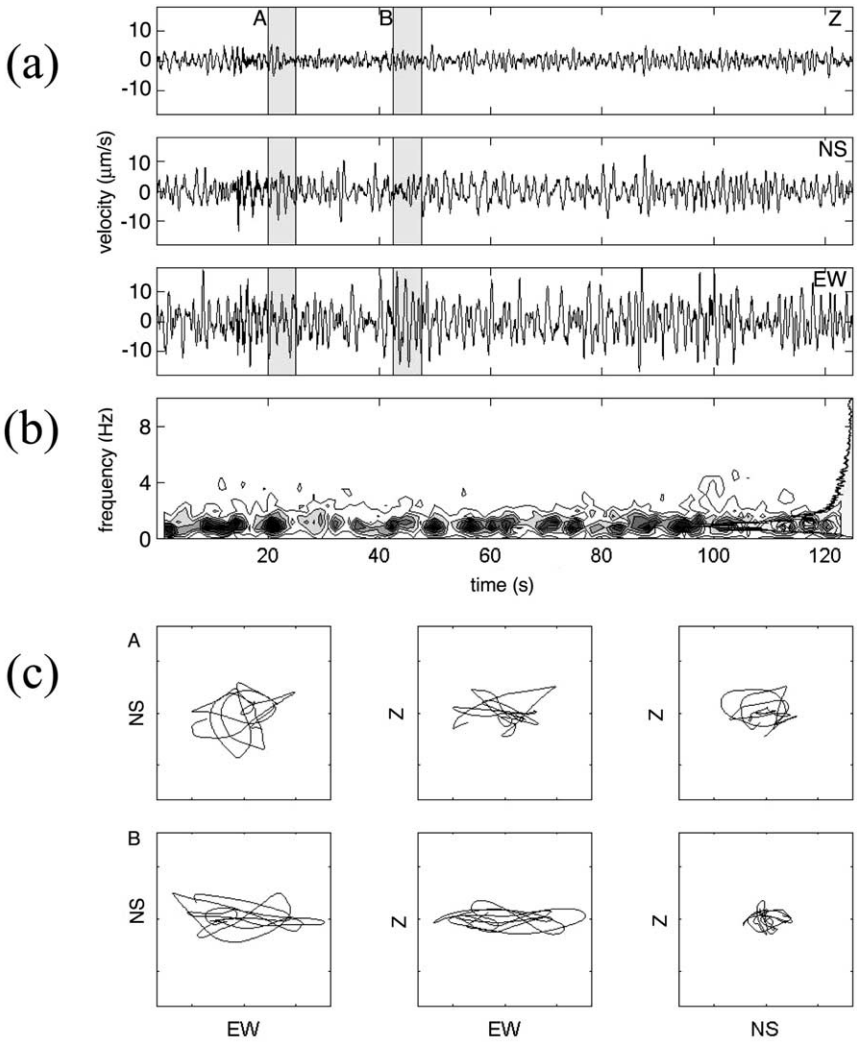

Fig. 5. Example of a tremor episode recorded at the Fumarole array. (a) Seismograms of the three components of ground motion. The gray areas labelled A and B correspond to two samples of waveforms. (b) Spectrogram of the vertical-component seismogram shown in (a). The vertical component is shown for comparison with the traces in previous figures. The right side of the plot shows the spectrum of the whole trace. (c) Particle motion diagram corresponding to the windows A and B in (a).

day. Using a lower limit of 30 events per day to declare a LP swarm (Ibáñez et al., 2000), there were nine swarms distributed randomly throughout the observation interval. This pattern coincides with that previously observed for the LP seismicity on the island (see fig. 4 of Ibáñez et al., 2000). The LP activity in 1998–1999 may therefore be considered normal for the area.

However, the situation is clearly different for VT earthquakes. During December 1998, only 8 VT were recorded. This earthquake occurrence rate is similar to the rate of a few tens of events per season reported by Ibáñez et al. (2000) for previous years. The pattern suddenly changed on January 4, 1999. There was a marked increase in the number of VT earthquakes recorded. The maximum activity was reached around January 20, with the occurrence of 80 VT earthquakes per day. When the field survey ended on February 25, the seismic activity was still high, often with

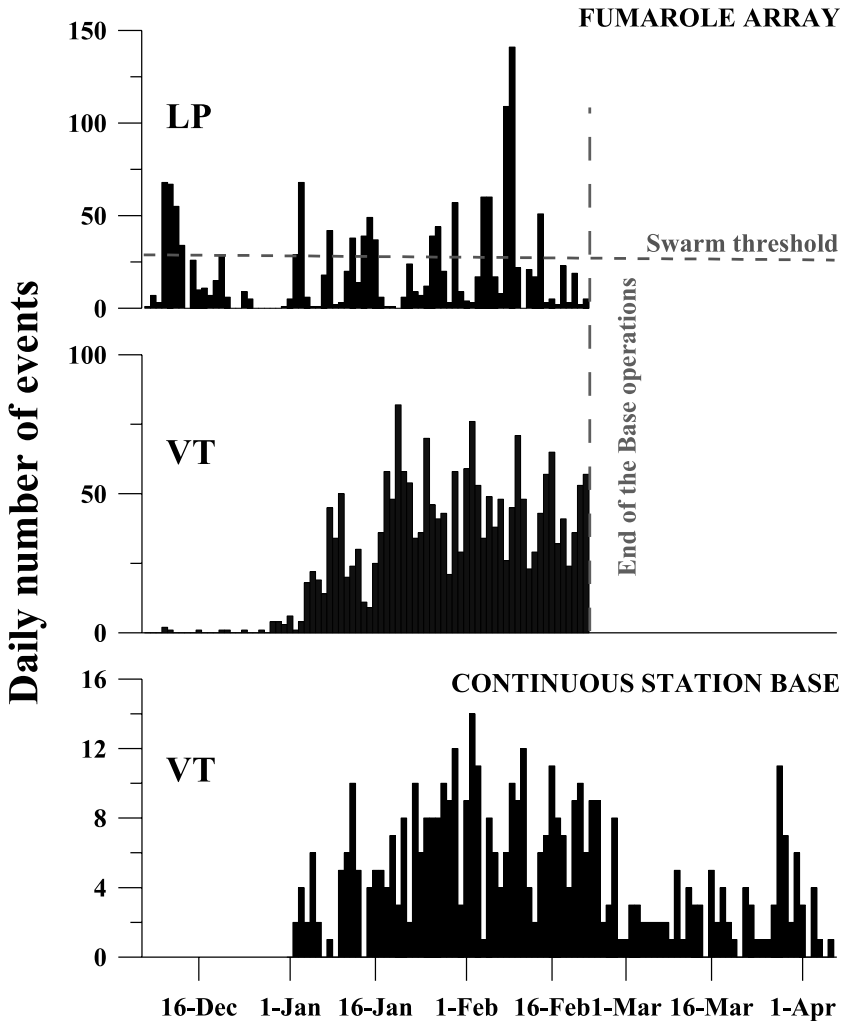

Fig. 6. Histogram of the daily number of LP events and VT earthquakes detected at the Fumarole array and the VT earthquakes recorded at the base continuous station between December 1998 and April 1999.

more than 50 earthquakes per day. At the bottom of Fig. 6, we also show a histogram of the VT earthquakes recorded by the continuous station deployed near the Spanish base, which operated for two more months. The generally lower number of earthquakes recorded by this station suggest that many of the events had magnitudes too low to exceed the detectability threshold at a station located only 2 km further to the south. From Fig. 6, we are not able to determine whether the activity was decreasing or not at the end of the recording period of the base station. The histogram gives no indication of a decrease. The activity may have lasted for some time after the control station stopped working. During the field season more than 3000 VT and LP earthquakes were recorded. Two of them were felt by the staff working on the island, one of them on January 11, at the beginning of the series, and one on January 20. This indicates a qualitative change in the seismic activity compared to the years 1992–1998. There were no reports of felt earthquakes since the 1991–1992 crisis (Ortiz et al., 1997).

About the time at which the first felt earthquake occurred, the properties of the volcanic

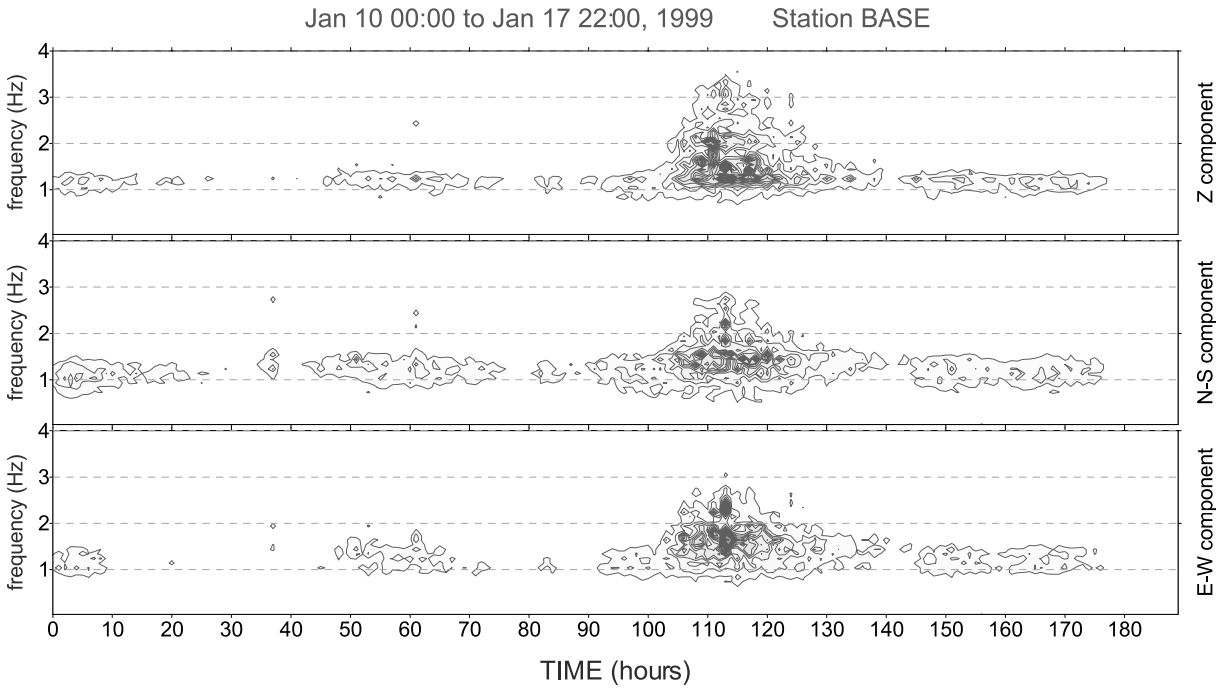

Fig. 7. Spectrogram of the three components of the ground motion recorded at the continuous base station between January 10 and 17, 1999.

tremor changed. Fig. 7 shows spectrograms of 180 h of tremor recorded at the continuous station near the Spanish base. On January 14 a period of 24 h of intense tremor was recorded, with a clear shift in frequency from 1 to 2 Hz. This period of tremor corresponds to a decrease of the number of VT and LP earthquakes in the histogram of Fig. 6. This is probably an artifact due to the reduced sensitivity of the antennas. The increase in the background amplitude affects the STA/LTA triggering algorithm.

Finally, only 15 hybrid events where identified during the field survey, all of them after the start of the VT earthquake series.

3. Array analyses

3.1. The Zero Lag Cross-Correlation method

In the present work we use the Zero Lag Cross-Correlation (ZLCC) technique (Frankel et al., 1991) to estimate the apparent slowness and back-azimuth of incoming wavefronts for successive time windows. Del Pezzo et al. (1997), Almendros et al. (1999) and Ibáñez et al. (2000) have given detailed discussions of the method and error estimation. The method is applied in the time domain and allows us to track the evolution of the source.

The method is based on the search of the apparent slowness vector which best fits the experimental data. It is solved using a grid search over the parameter space. The components of the apparent slowness (S_x, S_y) are allowed to range over an interval broad enough to include the actual solution. We use grid steps ΔS_x and ΔS_y, and for each step calculate the delay times for all stations and the corresponding average cross-correlation of the vertical components. The apparent slowness for which the maximum average cross-correlation (MACC) is reached represents the best fit to the propagation direction and velocity of the wavefront.

The procedure to perform the grid search was as follows. After inspecting the spectra, we se-

Table 1
Parameters used in the ZLCC procedure

Frequency band (Hz)	Length (samples)	Duration (s)	S_{max} (s/km)	ΔS (s/km)
1.0–3.0	300	1.5	4	0.04
3.0–5.0	100	0.5	4	0.04
1.0–4.0	200	1	4	0.04
4.0–8.0	80	0.4	1	0.01
8.0–12.0	60	0.3	1	0.01

lected the most energetic frequency band and filtered the seismograms using a zero-phase, four-pole, Butterworth band-pass filter. LP events and volcanic tremors were filtered in two frequency bands, 1–3 Hz and 3–5 Hz, while hybrids and VT earthquakes are filtered in three bands, 1–4 Hz, 4–8 Hz and 8–12 Hz. We used a moving window with a duration depending on the frequency band selected in order to contain approximately two periods of the signal (Table 1). On the basis of preliminary analyses, we restricted the grid search to adequate apparent slowness ranges which also depended on the frequency band. We selected a grid maximum and spacing of 4 and 0.04 s/km for frequency bands below 5 Hz, and 1 and 0.01 s/km, respectively, for higher frequency bands (Table 1). In each step the analysis window was shifted with 50% overlap, and the ZLCC technique was applied. For VT earthquakes, the analysis was restricted to the interval from the first P-wave to the early coda. For the other signals, the method was applied to the entire seismogram in order to find evidence of possible persistent sources, commonly observed in volcanic areas (e.g. Goldstein and Chouet, 1994).

3.2. LP events and tremor

The ZLCC method was applied to 350 LP events and volcanic tremor episodes recorded at the Fumarole array. We selected two frequency bands, 1–3 Hz and 3–5 Hz. For the 1–3 Hz band the MACC value lies between 0.7 and 0.9. The average apparent slowness is 0.8 s/km and the back-azimuths are stable at about 270°N (Fig. 8). In many cases the pre-event noise of the LP events is also correlated. It has the same apparent slowness and back-azimuth as the LP events but smaller MACC values, between 0.6 and 0.8. In the 3–5-Hz band we observe sporadic arrivals of correlated phases with MACC values greater than 0.7. Quite reasonably the apparent slownesses are higher than those for the 1–3-Hz band, with a peak between 2 and 2.5 s/km. Back-azimuth solutions point into several directions, the most important around 300°N (Fig. 8).

These distributions of apparent slowness and back-azimuth for the LP events and tremor are compatible with those observed by Ibáñez et al. (2000) for the same event types. Ibáñez et al. (2000) found that the LP seismicity at Deception Island during the 1995–1998 surveys was related to hydrothermal interactions between melting snow and ice and shallow hot material. Taking into account the similarity of waveforms and spectra, the coincidence of slowness distributions, and the fact that the main back-azimuth points to the location of glaciers close to the array, we are confident that the source mechanism suggested is applicable to the purely volcanic seismicity analyzed here.

3.3. VT earthquakes

A set of 1500 VT earthquakes recorded at the Fumarole array was selected on the basis of the signal-to-noise ratio of the first P-wave. They were analyzed in three frequency bands, 1–4 Hz, 4–8 Hz and 8–12 Hz. Between 1 and 3 Hz well correlated solutions were always observed, without any peak that could be related to the arrival of the P- or S-waves. For solutions with MACC values greater than 0.7, the distributions of apparent slowness and back-azimuth are very similar to those observed for LP events and tremor (Fig. 9). This suggests that the low-frequency signal, related to the LP events and tremor, is continuous and uncorrelated with the occurrence of earthquakes, which do not have much energy at these frequencies.

The situation changes when we look at solutions in the other two frequency bands. In this case there is only a short interval of well correlated waves with MACC values greater than 0.5. The remaining segments of the interval analyzed only have MACC values lower than 0.25. These

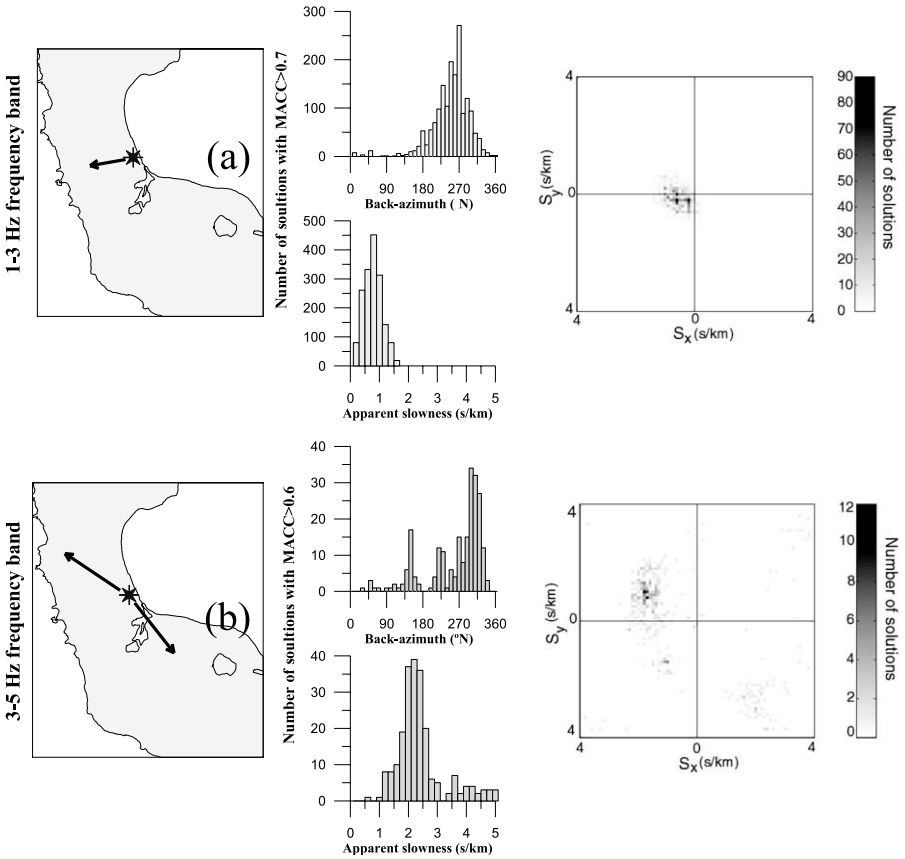

Fig. 8. Results of array analysis for the LP events and tremor in the 1–3-Hz (a) and 3–5-Hz (b) frequency bands. The histograms show the back-azimuths and apparent slownesses for the two frequency bands. The two-dimension plot represent the same values of the histograms with Sx (slowness) on the horizontal axis, Sy in the vertical and the number of solutions as level. Back-azimuth and apparent slowness can be derived easily from them. The arrows on the maps correspond to the apparent slowness vectors deduced from the ZLCC results.

peaks of MACC always coincide with arrivals of the P-wave. Since we use only vertical components, we did not find high MACC values corresponding to any S-wave arrival. Solutions for the 4–8-Hz and 8–12-Hz bands usually coincide and give very similar apparent slownesses and back-azimuths. For each earthquake we selected the apparent slowness and back-azimuth that provide the highest MACC, which corresponds to the P-wave arrival. To avoid low-quality solutions, we impose a MACC threshold of 0.5, which selected 863 earthquakes from the initial set of 1500. Fig. 10 shows histograms of the apparent slowness and back-azimuth for this set of earthquakes. The apparent slowness distribution is centered on 0.3 s/km, which is compatible with the arrival of body waves. The back-azimuth values are completely different from those observed for the LP seismicity. We can distinguish between at least two peaks of back-azimuth at 50 and 90°N, which both point toward Port Foster. Apparently, there is no relationship between the source of VT earthquakes and LP seismicity.

3.4. Hybrid events

From the 15 hybrid events detected, we selected nine for the analysis. They were analyzed in the frequency bands and with the parameters used for the VT earthquakes. In the low-frequency band

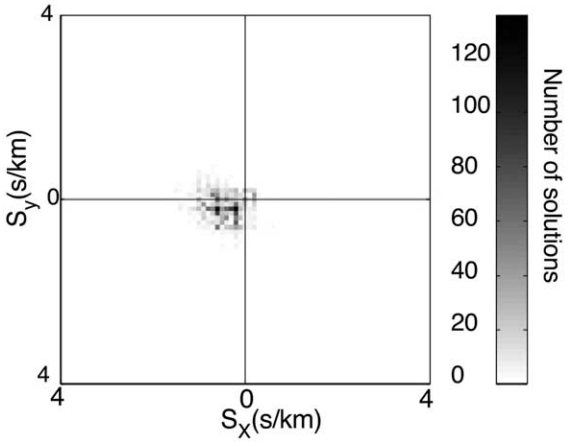

Fig. 9. The two-dimension plots representing the same values of the histograms with Sx (slowness) on the horizontal axis, Sy in the vertical and the number of solutions as level obtained during the analysis of the VT earthquakes in the 1–4-Hz frequency band.

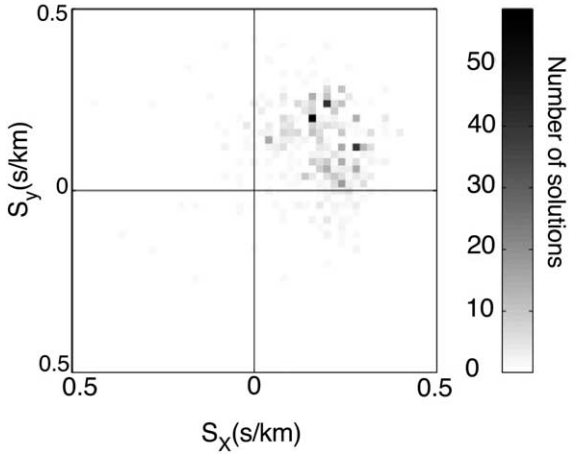

Fig. 10. The two-dimension plots representing the same values of the histograms with Sx (slowness) on the horizontal axis, Sy in the vertical and the number of solutions as level obtained for the P-wave arrival of each VT earthquake. The solutions correspond to the maximum values of MACC obtained in the 4–8-Hz and 8–12-Hz frequency bands.

solutions are usually well correlated, which indicates a stable source. Apparent slownesses are similar to those observed for the LP seismicity, with values centered on 0.6–0.8 s/km (Fig. 11). However, even though the low-frequency part of a hybrid resembles a LP event, the distribution of back-azimuths for hybrids is completely different from that observed for the LP seismicity. They coincide instead with the directions obtained for the high frequency bands in the analysis of the VT earthquakes.

For the high frequency bands, well correlated solutions only appear at the P-wave onset, as in the case of VT earthquakes (see Table 2). Slowness values and back-azimuths are also similar to the solutions obtained for the VT earthquakes, as are the estimates of the S–P delays.

4. Source location

4.1. LP and tremor source

We cannot determine the distance to a source of LP seismicity with a single seismic antenna, unless the distance is small compared to the array aperture and the circular wavefront approximation can be used (Almendros et al., 1999). There is some evidence that the source area could indeed

Table 2
Array solutions for the hybrid events

Date (day-month) 1999	Time (hh:mm) GMT	S–P (s)	Back-azimuth (°N)	Apparent slowness (s/km)	MACC
13-Jan	09:24	0.72	81	0.37	0.90
15-Jan	11:27	0.76	56	0.22	0.86
17-Jan	14:29	0.85	81	0.37	0.85
20-Jan	12:32	0.90	122	0.31	0.73
26-Jan	20:02	1.16	72	0.26	0.84
27-Jan	20:31	1.12	66	0.20	0.93
28-Jan	06:44	1.16	67	0.26	0.84
28-Jan	21:52	1.29	72	0.25	0.95
16-Feb	17:32	1.33	105	0.23	0.78

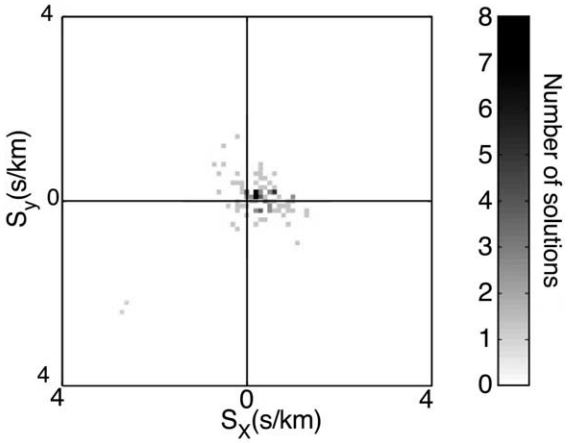

Fig. 11. The two-dimension plots representing the same values of the histograms with Sx (slowness) on the horizontal axis, Sy in the vertical and the number of solutions as level obtained during the analysis of the hybrid events in the 1–4-Hz frequency band.

be very near the array. For example, the LP activity is only recorded by the sensors of the array, and not by nearby seismic stations less than 1.5 km away. In the same way, LP seismicity recorded at the continuously recording station near the Spanish base is not detected at Fumarole array. In both cases the amplitudes of the signals are similar. Using this energetic argument we conclude that the sources of LP events and tremor recorded at the array are less than 1.5 km away.

4.2. VT earthquakes and hybrids

Hypocenter locations of VT earthquakes and hybrids can be determined accurately using the apparent slowness, back-azimuth, and S–P time. The S–P time fixes the distance to the source, the back-azimuth is the direction to the epicenter and the apparent slowness provides the incidence angle. We use inverse ray tracing through a velocity model for Deception Island (Table 3). This model is a combination of the models proposed by Ibáñez et al. (2000) and Saccorotti et al. (2001), and smoothed using a fourth-degree depth-dependent polynomial. In this way, we determine the location for both VT earthquakes and hybrid events given in the hypocentral map in Fig. 12.

Errors in the locations are derived from the errors in the array parameters and the S–P time. Following Del Pezzo et al. (1997), the average errors in the apparent slowness and back-azimuth are ±10% of the measured apparent slowness and ±7° of the back-azimuth, respectively. The average error in the determination of the S–P time is about ±0.05 s. Using these limits to perturb the original apparent slowness, back-azimuth, and S–P time for input to the ray tracing procedure, we delimit a region around the estimated hypocenter giving the error in the location of the source. For example, using average values of 0.8 s/km for the apparent slowness, 90°N for the back-azimuth, and 1.0 s for the S–P delay, we obtain a region of about $0.5\times0.5\times0.5$ km^3. Errors of this size are typical and imply that we should not interpret the detailed structure of the hypocentral distribution shown in Fig. 12, but only its general properties. The choice of velocity model also affects the results. We have tested other models, and conclude that for realistic models the source locations do not differ enough to change our interpretation of the seismicity.

The hypocentral distribution for the VT earthquakes and hybrids shown in Fig. 12 indicates that the seismicity is clustered at a focal depth of around 2 km near the array and toward the northeast. More than 90% of the events are clustered in a volume of around 10 km^3. However, deeper and more distant events have also been located, with focal depths reaching 10 km and epicentral distances up to 18 km. The cluster has two main arms. The first one extends about 3 km N45°E, with focal depths between 1 and 4 km. The second arm is longer but more diffuse, and extends N80°E. In any case the seismicity is all located within the inner bay of Deception Is-

Table 3
Velocity structure for Deception Island

Z (km)	*Vp* (km/s)	*Vp*/*Vs*
0.04	0.9	1.80
1.96	2.30	1.77
6	4.5	1.73
12.0	6.0	1.73
∞	8.0	1.73

Z = layer thickness; *Vp* = P-wave velocity; *Vs* = S-wave velocity.

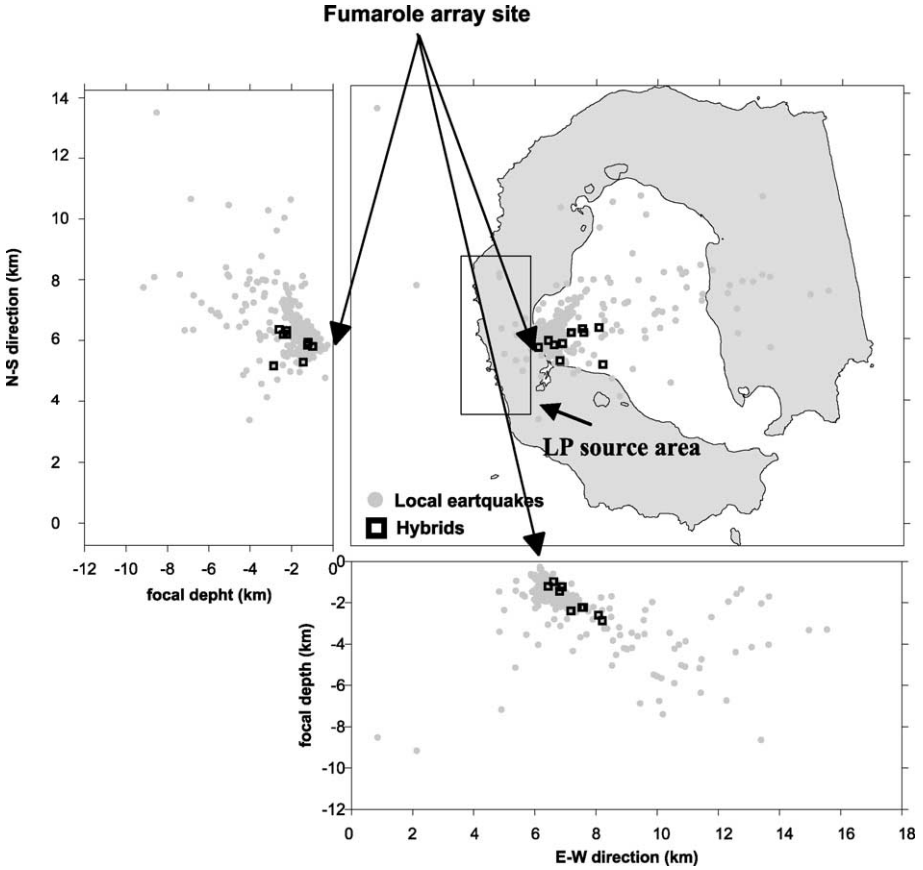

Fig. 12. Hypocentral locations of the VT earthquakes (dots) and hybrid events (squares). The box over Deception Island shows the possible source region for LP seismicity.

land and apparently dips with an angle of about 45°. Hybrid event locations coincide with the cloud of VT earthquake. Most of them are contained in the branch of seismicity extending toward N80°E.

To study the migration of hypocenters with time, we divide the seismic series by time windows, and plot the hypocentral locations in each window separately (Fig. 13). Initially the sources are concentrated in a small region between depths of 1 and 2 km. As time progresses we observe that the source volume increases in size, mainly to greater depths, forming between 1 and 3 km depth and with 2 km of horizontal extension. At the same time the events migrate downward. The deeper and more distant seismicity expressed itself in the larger S–P times, that reached values between 1 and 3 s. The two felt earthquakes were located in the center of the main focal volume.

5. Energetic characterization of the seismic series

In this section we quantify the size of the VT earthquakes. One possible measure is the moment-magnitude scale. The moment-magnitude was defined by Kanamori (1977) as:

$$M_w = 2/3 \log M_o - 6.06 \quad (1)$$

where the moment is measured in Nm.

In this expression M_o corresponds to the seismic moment which can be expressed by:

$$M_o = (\Omega_o / \Psi_{\theta\phi})\,(4\pi\rho v_s^3 R) \quad (2)$$

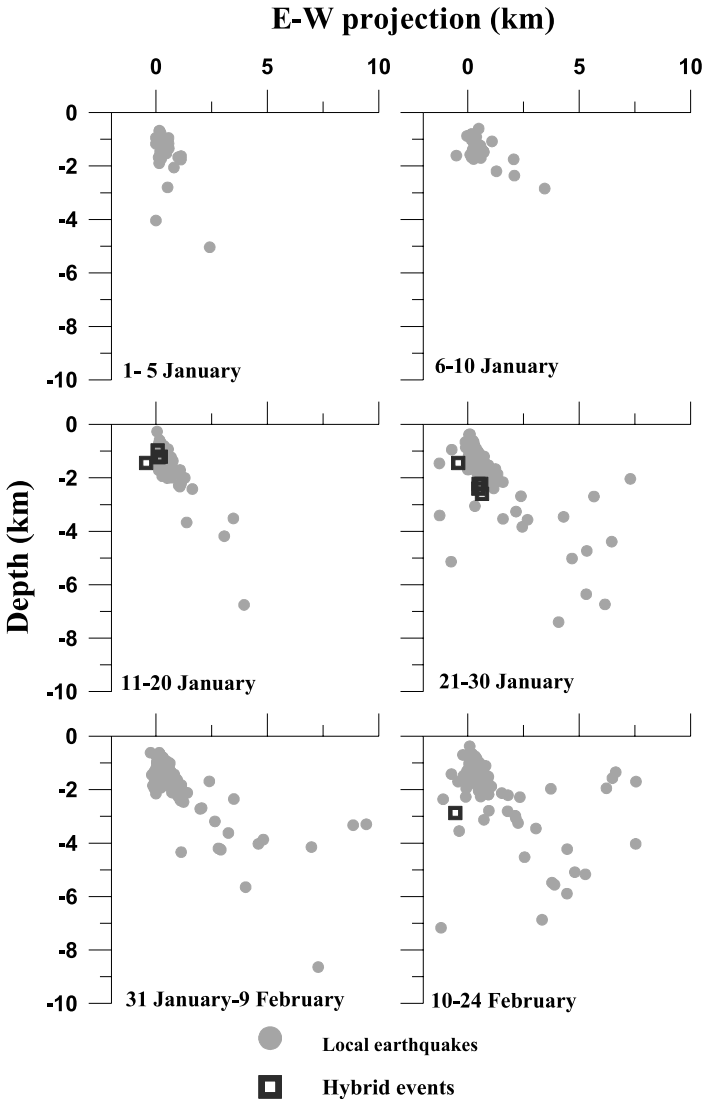

Fig. 13. Evolution of the source locations of the VT earthquakes and hybrid events with time. The panels show hypocentral depth and EW projection during six time intervals.

Ω_o is the spectral level of the attenuation-corrected displacement spectrum which remains flat until the corner frequency f_o; $\Psi_{\theta\phi}$ is a function accounting for the body-wave radiation pattern and the effect of the free surface (we assume a value of 0.85); R is the hypocentral distance; v_s is the S-wave velocity and ρ is the density of the medium.

To estimate Ω_o and f_o we can use both P-waves and S-waves, but it is more correct to use only the S-wave displacement spectrum. As the original Brune model (Brune, 1970) assumed SH-waves, we should use horizontal components for these estimates. The attenuation-corrected spectrum is obtained applying the Q factor to the ground displacement spectrum. The Q factor, the quality factor of the medium, is directly related to seismic attenuation in the region between source and re-

Table 4
Parameters used in the moment-magnitude determination

Hipocentral distance (km)	Q-factor	S-wave velocity (km/s)
<1	50	1
$1<D<1.5$	60	1.2
$1.5<D<2$	80	1.5
$2<D<4$	150	1.8
$D>4$	260	2.5

ceiver. We used frequency-independent Q values obtained as a function of the distance from the study of Martínez-Arévalo et al. (2003), (Table 4).

Other parameters necessary for the estimation of M_o are the density of the medium and body wave velocity. We assume an average density of 2.7 g/cm^3, and velocity values averaged from Table 3 (see Table 4).

The S-wave spectra were calculated using a MATCAD© package. To determine of the spectrum of the ground displacement, we use a 2.56-s window starting at the S-wave onset. We chose data from the three-component station of the Fumarole array which had the best signal-to-noise ratio, and averaged the two horizontal S-wave spectra. The level of the flat part of the spectrum and the corner frequency were determined using a minimization algorithm starting from a initial value for corner frequency, with the frequency decay fixed to -2. From the spectrum we also determine the stress drop, seismic moment, moment magnitude and the probable source radii using two possible hypotheses, Madariaga's model (Madariaga, 1977) and Brune's model (Brune, 1970). We applied this study to most of the VT earthquakes. The biggest ones were excluded because their S-waves were saturated in the recording. For this small data set (6 events) we used the same procedure at a more distant station, the broad-band station located at the Spanish base 'Juan Carlos I' (Livingston Island), 45 km north of Deception Island. In this case we used different parameters to correct the spectra. The S-wave velocity was 3.0 km/s and, because there is no attenuation model for the region, we used Q determined for Granada from Ibáñez et al. (1990), $Q=90\ (f/f_o)^{0.85}$. For this epicentral distance, the possible error introduced by the uncertainty in the Q value is a second order effect, because the geometrical spreading correction is more important.

The 863 earthquakes span a magnitude range from -0.8 to 3.4. The magnitudes of the VT earthquakes allow us to follow the evolution of the energy of the seismic series, as well as estimate the cumulative seismic moment (Fig. 14). Except for the two earthquakes of magnitude 2.8 and 3.4, the energy release as a function of time is more or less steady. The distribution of magnitudes is nearly the same throughout the series.

The stress drop of the seismic series derived from the magnitude analysis is very low (Fig. 15), with more than 95% of the values concentrated between 0.1 and 4 bar. The corner frequencies range from 40 Hz for the smallest events to 6 Hz for the biggest ones (not including the events which saturated the records). The relationship between corner frequency and magnitude possibly

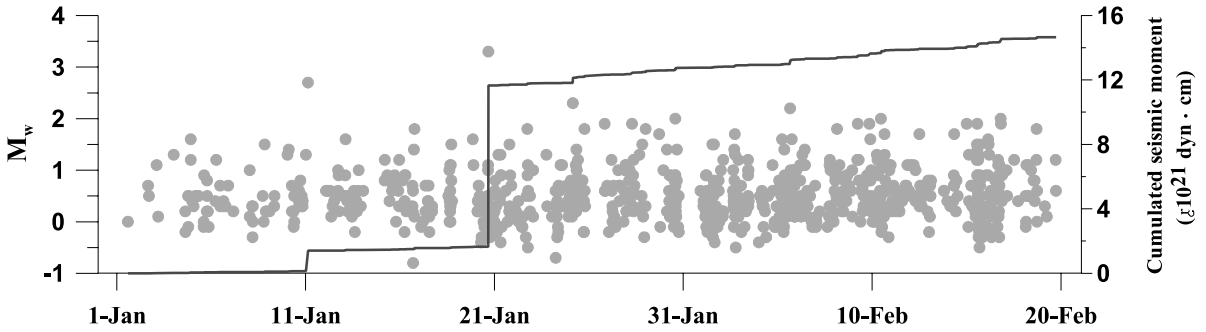

Fig. 14. Earthquake magnitude (left axis) vs. time during January–February, 1999. The solid line represents the cumulative seismic moment (right axis).

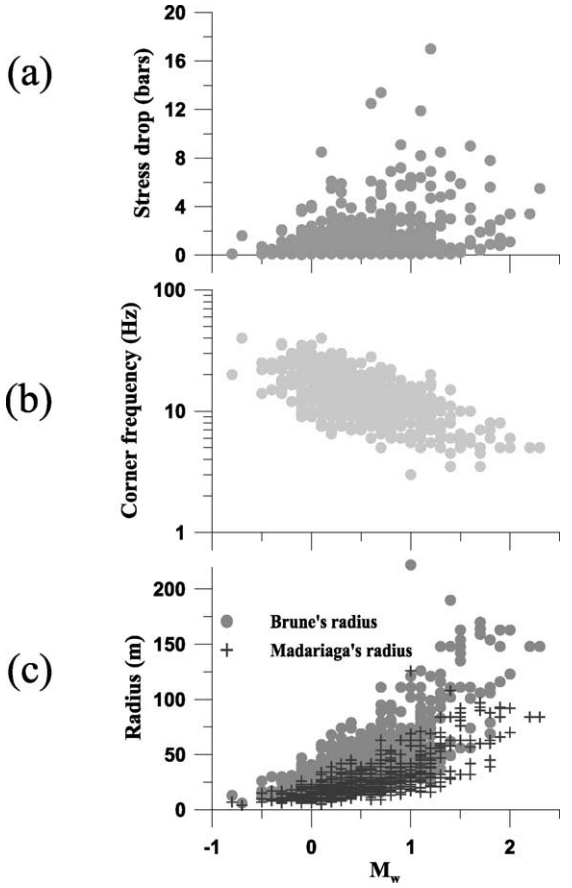

Fig. 15. Stress drop (a), corner frequency (b), and source radius (c) vs. magnitude for the VT earthquakes analyzed.

reflects a scaling law for the series, but the data are too dispersed to obtain a significant fit. The high values of the corner frequencies are consistent with the spectra of the VT earthquakes, which have high signal-to-noise ratios up to frequencies of 50 Hz. The source radii derived from the spectral analysis reveal the small dimensions of the source (Fig. 15). Using Brune's model we found that the source dimensions range from 10 to up to 200 m, with an average of 50 m. In the case of Madariaga's model the dimensions are smaller, ranging from 5 to 120 m, with an average value of 30 m.

In Fig. 12 we observe that the seismicity is clustered close to the array. We can investigate whether this cloud of data could be an artifact due the detection threshold of the seismic instruments. To do this we plot the moment magnitude vs. focal depth and epicentral distance (Fig. 16a). We can see that all earthquakes with magnitudes smaller than about 0.8 are concentrated in the first two km of focal depth and epicentral distance. For more distant events, the minimum magnitude detected is around 1.0. This implies that there might be low-magnitude seismicity located more than 2 km from the array which cannot be detected. Thus, the observed clustering of the seismicity observed in Fig. 12 could be an artifact. The real distribution of seismicity could be quite different. In fact, if we represent only events with magnitudes greater than 1.2, the clustering is reduced and the hypocenter cloud extends clearly to the east and northeast of the array (Fig. 16b).

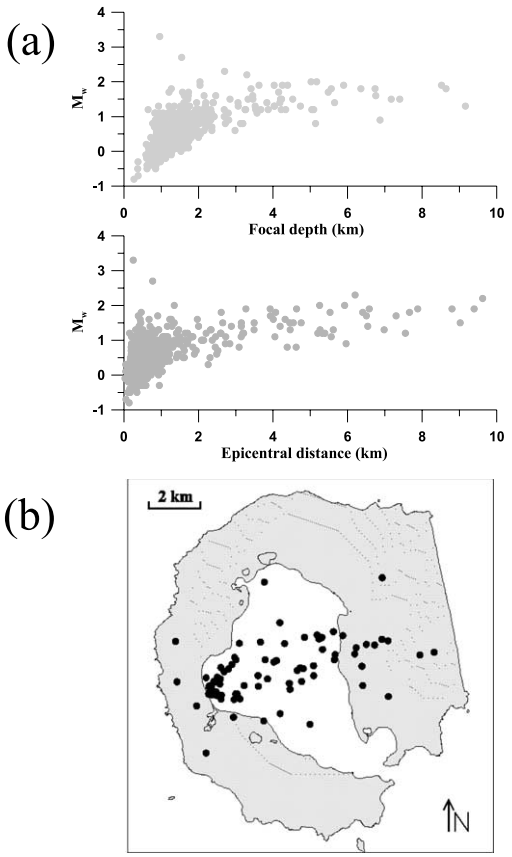

Fig. 16. (a) Plots of the VT earthquake magnitude vs. focal depth and epicentral distance. (b) Epicentral plot for VT earthquakes with magnitudes greater than 1.2.

6. Evidence of different source processes

The source dimensions indicate the small size of the fractures involved in the events of the seismic series. These small fractures are primarily concentrated in a small focal volume, inside of which we detected hundreds of events. Without a seismic network we are not able to estimate the focal mechanisms. However several observations allow us to distinguish at least the presence of many distinct source mechanisms.

Visual analysis of the VT earthquake records reveals clear differences between events which have similar source locations, for example in the direction and shape of the first P-wave motions. Fig. 17 shows two events with similar apparent slownesses, back-azimuths, and S–P times. Although their sources must be located close together, the polarities of the first pulse and whole seismograms are different. This could indicate that the source mechanisms are different. We measured the polarities of the first motion for earthquakes with impulsive arrivals. In Fig. 18 we present the source locations in different time intervals for events with clear up or down first motion directions. There are no obvious spatial or temporal differences between the two distributions.

Another piece of evidence indicating the complexity of the source region is the occurrence of multiplets of events. Several conditions are necessary for the repeated generation of similar earthquakes. Since the path and site effects are essentially the same for earthquakes with nearby hypocenters, the events must have the same source-time function and source mechanism. The presence of multiplets is important because the similarities among waveforms allow phase onsets to be determined with high consistency. This can lead to an improvement in the quality of the hypocentral locations. To identify earthquake multiplets we used the method proposed by Saccorotti et al. (2002) in their study of the Agron series in Southern Spain. In this way we obtained several tens of families, usually with more than 10 events per family. Fig. 19 shows examples of two families. Earthquakes of each family are located within a very small volume. However, they do not appear to correlate in time. There are intervals of several days or weeks between them. During these intervals, events with other source mechanisms often occur in the same source region. The presence of earthquake families in this seismic series is a very interesting topic that will be the subject of a future study.

7. Discussion

7.1. VT earthquakes and hybrids

To understand a fracture process with low stress drop, small dimensions and occurrence of multiplets, we can invoke the role of the fluids. In this framework the release of seismic energy is associated with lubrication of a pre-existing zone of weakness by fluids. Lubrication reduces the friction coefficients and decreases the effective

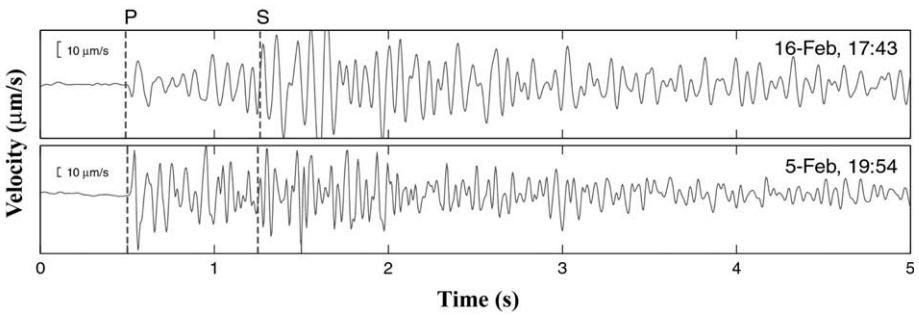

Fig. 17. Vertical-component seismograms of two VT earthquakes with very similar hypocenter locations. The labels P and S show the arrival of the P-waves and S-waves, respectively. The top record has a 'down' first motion, while the bottom record shows a clear 'up' first motion.

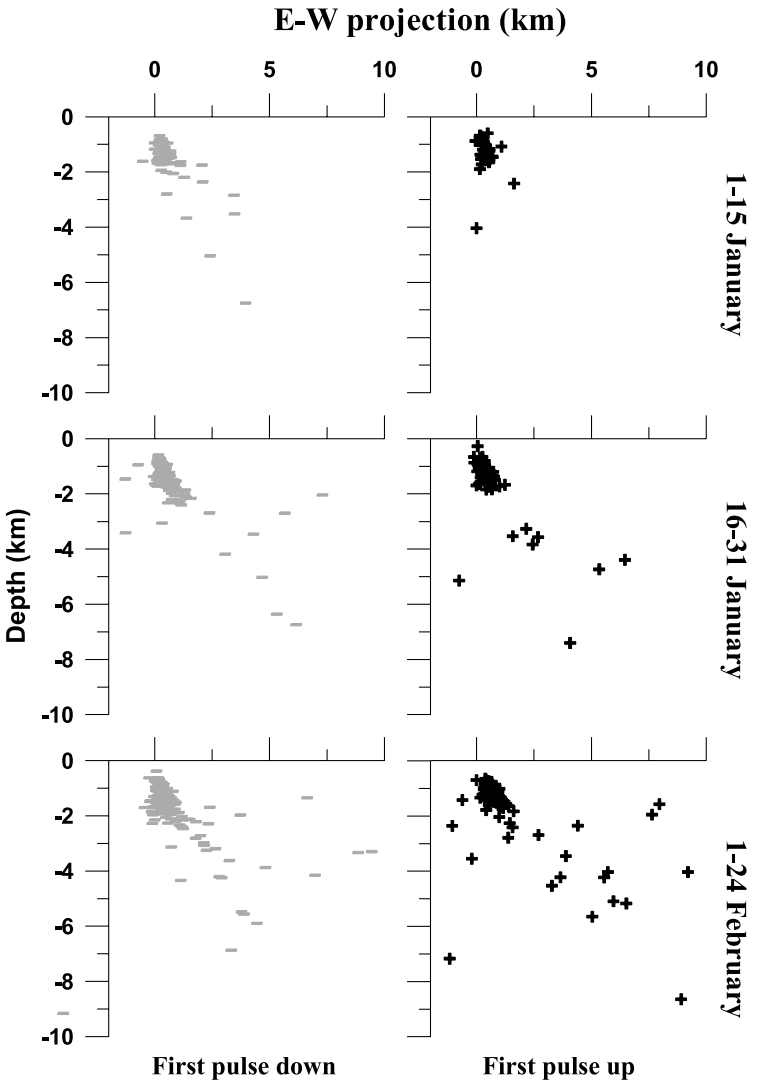

Fig. 18. Hypocentral distributions of VT earthquakes with clear down (left) or up (right) first motions. The top, center, and bottom rows correspond to different time periods.

normal stress over the fault surface. This can in turn trigger the earthquake.

During the seismic series some hybrid events were recorded. We are confident that the hybrids can be considered as true hybrids in the sense of the classification by Lahr et al. (1994): a volcano-tectonic earthquake plus a LP event. There are several observations that support this conclusion. For example, in the high frequency signal we are able to distinguish the arrival of P-waves and S-waves. The array solutions at high frequencies coincide with those obtained for the VT earthquakes. The azimuths of the LP part of the hybrid events point towards the inner bay, as the VT earthquakes do, not to the southeast as do the azimuths of the pure LP events and the tremor. In addition, the hypocenters of the initial earthquake of the hybrid events are located in the same area as the VT earthquakes. We can disregard the fact that the low-frequency wave package may

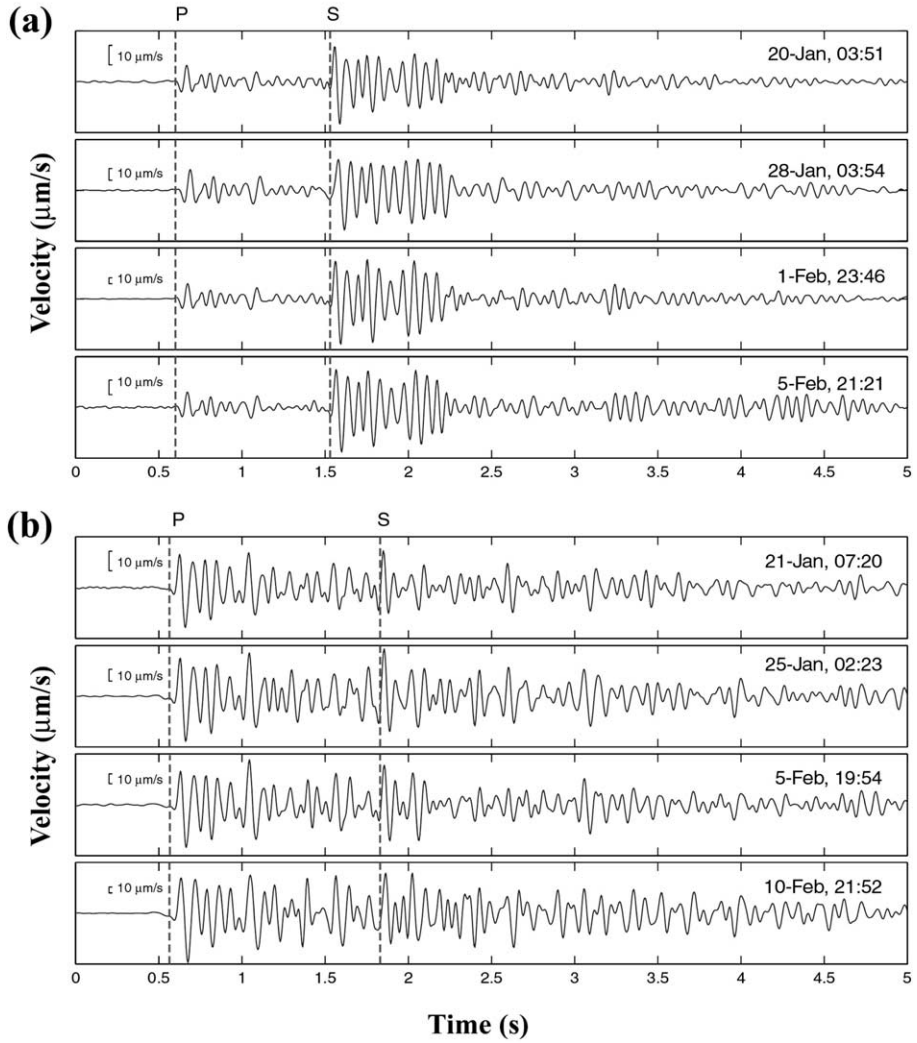

Fig. 19. Examples of two families of VT earthquakes with S–P times of ~0.8 s (a) and 1.3 s (b).

have originated as a path or site effect, because we see earthquakes located very near to the hybrids that do not have this low-frequency train. The occurrence of hybrids during the seismic series is confirmation of the presence of fluids in the source area. These events are evidence that fluids are present in the fracture systems. It is important to point out that the hybrids were detected when the hypocenters of the VT earthquakes began to migrate downwards. This observation is important for understanding the process controlling the seismic series.

7.2. Hypothesis about the origin of the series

Based on the volcanic nature of Deception Island and the well known effects of the regional tectonics on the island (Pelayo and Wiens, 1989), we can imagine three possible scenarios for the source of the stress disturbance producing the series of VT earthquakes. First, these events could be a classical tectonic seismic swarm caused by regional stress. Second, they may be a seismic swarm produced directly by the movement of magma through the source region. Third, the seis-

mic series may be caused by stress generated by the uplift of the source area due to the injection of magma in depth.

We may exclude the first scenario, because the seismic activity is restricted to the inner bay and there are no earthquakes outside the island. If the series were induced by regional stresses, there should be activity along the faults that cross the island (Martí et al., 1996), which we did not detect. Moreover, it is difficult to be convinced that the regional stress field could trigger the seismic series in a single shallow point inside the island. The behavior of the series is not that of a typical main shock–aftershock sequence. The variety of source mechanisms involved in such a small focal volume, the repeated rupture of some fault planes implied by the earthquake multiplets, and the low stress drop, indicate that the source region could be characterized by a complex stress distribution and an asymmetrical pattern of small microfaults. On the other hand, Legrand et al. (2002) have calculated the stress tensor below the Guagua Pichincha volcano (Ecuador) obtaining a single stress tensor but with a mixture of normal faults and strike-slip component faults. These authors have found that the presence of different focal mechanisms could be compatible with a unique stress tensor.

It is unlikely that magmatic fluids are directly involved. If this were the case, we should have observed an upward migration of the hypocenters, following the upward migration of magma. To the contrary, we observed a downward migration of hypocenters. The occurrence of similar events, separated by several days or weeks, is not compatible with this hypothesis. The presence of multiplets reflects that the stress triggering of the earthquakes is nearly constant with time. In contrast, a migration of magma should produce an evolution of the stress field. Further evidence against this hypothesis comes from the separate source areas in which the LP seismicity and the VT earthquake activity are located. The presence of magma at shallow depth and relatively low pressure are usually accompanied by gas, which produces LP and tremor seismicity (e.g. Fehler, 1983; Gil Cruz and Chouet, 1997). The fact that the LP source area and the earthquake hypocentral region do not coincide implies that there is no magma at shallow depth at any time during the series.

Thus, the best model for explaining the origin of the seismic series is the uplift of the Port Foster area by a deep magmatic injection. The presence of a magma reservoir in the Northeast area of Port Foster has been reported by several authors (Blanco, 1997, García et al., 1997). An increase of pressure within the magma reservoir, or the upward displacement of magma, perturbs the stress field in the region over the reservoir. When the stress reaches a threshold value, fracture processes begin, following pre-existing zones of weakness and the series becomes fully active. The absence of visible evidence of a subsequent eruption and the lower level of earthquake activity observed since 1999 lead us to think that the injection of magma stopped before reaching the vicinity of the surface. The uplift hypothesis is compatible with the majority of the observations derived from the present analysis.

We have found that most VT earthquakes were the consequence of small stress drop changes (less than 4 bar) on fractures with an average radius of about 50 m. This fact may be explained by lubrication of the microfaults due to pressurized fluids. The increase of pore pressure in the very shallow crust overlying the magmatic system could have induced the repeated activation of the fracture network. The presence of fluids in the source area not only expedites the fracture processes, but also explains the origin of the hybrids observed. Their low-frequency segments are produced by resonances of fluid-filled cracks. The fluid involved in the lubrication of the microfaults and the generation of hybrid events is probably not magmatic, as explained above, but water embedded in the geological structure. Martini and Giannini (1988) reported the existence of a shallow aquifer near the epicentral area, and a deeper aquifer may be present as well (Martini and Casselli, pers. commun.).

The process described in the present analysis does not seem to be rare at Deception Island. The seismic crisis occurring in 1992 has been described in similar terms (Ortiz et al., 1997). This means that in seven years we observed two vol-

canic crises. If we take into account that there are no permanent stations in the island, and that we are able to make measurements during three months every year (from December to February), then similar intervals of high seismic activity may be occurring more often than we have observed. Deception Island, therefore, seems to be a very active volcano. However, it is also a volcano frequently visited by scientific teams and thousands of tourists, especially during the summer season. In order to reduce the risk associated with volcanic hazards, we must put greater effort into seismic and geophysical monitoring of Deception Island.

Acknowledgements

This work was partially supported by projects ANT98-1111, REN-2000-2897, e-Ruption, and REN-2001-3833. We thank J. A. Peña for his invaluable help in the field work; B. Chouet, J. Morales, G. Alguacil, and C. Martínez-Arévalo for useful comments on the manuscript; Margaret Hellweg for her very useful comments and great grammatical corrections that have improved the paper; Denis Legrand for his valuable comments to the manuscript; the staff and scientists of the Gabriel de Castilla Base; and F. Calexico for his moral support. Logistical support was provided by the Spanish 'Ejército de Tierra' and 'Armada'.

References

Almendros, J., Ibanez, J.M., Alguacil, G., Del Pezzo, E., 1999. Array analysis using circular wavefront geometry: An application to locate the nearby seismo-volcanic source. Geophys. J. Int. 136, 159–170.

Almendros, J., Chouet, B., Dawson, P., Bond, T., 2002. Identifying elements of the plumbing system beneath Kilauea Volcano, Hawaii, from the source locations of very-long-period signals. Geophys. J. Int. 148, 303–312.

Benoit, J.P., McNutt, S.R., 1996. Global volcanic earthquake swarm database and preliminary analysis of volcanic earthquakes swarm duration. Ann. Geofis. 39, 221–229.

Blanco, I., 1997. Análisis e interpretación de las anomalías magnéticas de tres calderas volcánicas: Decepción (Shetland del Sur, Antátida), Furnas (San Miguel, Azores) y las Cañadas del Teide (Tenerife, Canarias). Ph.D. Thesis, Universidad Complutense de Madrid, 250 pp.

Brune, J.N., 1970. Tectonic stress and the spectra of seismic shear waves. J. Geophys. Res. 89, 1132–1146.

Chouet, B., 1988. Resonance of a fluid-driven crack: Radiation properties and implications for the source of long-period events and harmonic tremor. J. Geophys. Res. 93, 4375–4400.

Chouet, B., 1992. A seismic model for the source of long-period events and harmonic tremor. In: Aki, K., Gasparini, P., Scarpa, R. (Eds.), Volcanic Seismology. IAVCEI Proceedings in Volcanology 3, Springer, pp. 133–156.

Chouet, B., 1996. Long-period volcano seismicity: Its source and use in eruption forecasting. Nature 380, 309–316.

Chouet, B.A., Page, R.A., Stephens, C.D., Lahr, J.C., Power, J.A., 1994. Precursory swarms of long-period events at Redoubt Volcano (1989–1990), Alaska: Their origin and use as a forecasting tool. J. Volcanol. Geotherm. Res. 62, 95–135.

Crosson, R.S., Bame, D.A., 1985. A spherical source model for low-frequency volcanic earthquakes. J. Geophys. Res. 90, 10237–10247.

Dahm, T., 1992. Numerical studies of the dynamics of fluid-filled cracks placed in series: A model for inharmonic peaked tremor spectra. In: Aki, K., Gasparini, P., Scarpa, R. (Eds.), Volcanic Seismology. IAVCEI Proceedings in Volcanology 3, Springer, pp. 190–200.

Del Pezzo, E., La Rocca, M., Ibanez, J.M., 1997. Observations of high-frequency scattered waves using dense arrays at Teide volcano. Bull. Seismol. Soc. Am. 87, 1637–1647.

Fehler, M., 1983. Observations of volcanic tremor at Mount St. Helens volcano. J. Geophys. Res. 88, 3476–3484.

Frankel, A., Hough, S., Friberg, P., Busby, R., 1991. Observations of Loma Prieta aftershocks from a dense array in Sunnyvale, California. Bull. Seismol. Soc. Am. 81, 1900–1922.

García, A., Blanco, I., Torta, J.M., Astiz, M.M., Ibáñez, J.M., Ortiz, R., 1997. A search for the volcanomagnetic signal at Deception volcano (South Shetland I. Antarctica). Ann. Geofis. 40, 319–327.

Gil Cruz, F., Chouet, B., 1997. Long-period events, the most characteristic seismicity accompanying the emplacement and extrusion of a lava dome in Galeras volcano, Colombia, in 1991. J. Volcanol. Geotherm. Res. 77, 121–158.

Goldstein, P., Chouet, B., 1994. Array measurements and modeling of sources of shallow volcanic tremor at Kilauea Volcano, Hawaii. J. Geophys. Res. 99, 2637–2652.

Hellweg, M., 2000. Physical model for the source of Lascar's harmonic tremor. J. Volcanol. Geotherm. Res. 101, 183–198.

Ibáñez, J.M., Del Pezzo, E., De Miguel, F., Herraiz, M., Alguacil, G., Morales, J., 1990. Depth dependence seismic attenuation in Granada zone (South Spain). Bull. Seismol. Soc. Am. 80, 1232–1244.

Ibáñez, J.M., Del Pezzo, E., Almendros, J., La Rocca, M., Alguacil, G., Ortíz, R., García, A., 2000. Seismovolcanic signals at Deception Island volcano, Antarctica: Wave field analysis and source modeling. J. Geophys. Res. 105, 13905–13931.

Julian, B.R., 1994. Volcanic tremor: Nonlinear excitation by fluid flow. J. Geophys. Res. 99, 11859–11877.

Kanamori, H., 1977. The energy release in great earthquakes. J. Geophys. Res. 82, 2981–2987.

Klein, F.W., Koyanagi, R.Y., Nakata, J.S., Tanigawa, W.R., 1987. The seismicity of Kilauea's magma system. In: Decker, R.W., Wright, T.L., Stauffer, P.H. (Eds.), Volcanism in Hawaii. US Geol. Surv. Prof. Pap. 1350, pp. 1019–1085.

Koyanagi, R.Y., Chouet, B.A., Aki, K., 1987. Origin of volcanic tremor in Hawaii, Part I. In: Decker R.W., Wright, T.L., Stauffer, P.H. (Eds.), Volcanism in Hawaii. US Geol. Surv. Prof. Pap. 1350, pp. 1221–1257.

Kumagai, H., Chouet, B., 2000. Acoustic properties of a crack containing magmatic or hydrothermal fluids. J. Geophys. Res. 105, 25493–25512.

Lahr, J., Chouet, B., Stephens, C., Power, J., Page, R., 1994. Earthquake classification, location and error analysis in a volcanic environment: Implications for the magmatic system of the 1989–1990 eruptions at Redoubt volcano, Alaska. In: Miller, T., Chouet, B. (Eds.), The 1989–1990 Eruptions of Redoubt Volcano, Alaska. J. Volcanol. Geotherm. Res. 62, 137–151.

Legrand, D., Calahorro, A., Guillier, B., Rivera, L., Ruiz, M., Villagómez, D., Yepes, H., 2002. Stress tensor analysis of the 1998–1999 teconic swarm of northern Quito related to the volcanic swarm of Guagua Pichincha volcano, Ecuador. Tectonophysics 344, 15–36.

Madariaga, R., 1977. High-frequency radiation from crack (stress drop) models of earthquakes faulting. Geophys. J. R. Astron. Soc. 51, 625–652.

Martí, J., Vila, J., Rey, J., 1996. Deception Island (Bransfield Strait, Antarctica): An example of volcanic caldera developed by extensional tectonics. In: McGuire, W., Jones, A., Neuberg, J. (Eds.), Volcano Instability on the Earth and Other Planets. Geol. Soc. Spec. Publ. 110, pp. 253–265.

Martínez-Arévalo, C., Bianco, F., Ibáñez, J.M., Del Pezzo, E., 2003. Shallow seismic attenuation in the short period range of Deception Island volcano (Antarctica). J. Volcanol. Geotherm. Res. 128, this issue (DOI: 10.1016/S0377-0273(03)00248-8.

Martini, M., Giannini, L., 1988. Deception Island (South Shetlands): An area of active volcanism in Antarctica. Mem. Soc. Geol. Ital. 43, 117–122.

Nakano, M., Kumagai, H., Kumazawa, M., Yamaoka, K., Chouet, B., 1998. The excitation and characteristic frequency of the long-period volcanic event: An approach based on an inhomogeneous autoregressive model of a linear dynamic system. J. Geophys. Res. 103, 10031–10046.

Narváez, L., Torres, R.A., Gómez, D.M., Cortés, G.P., Cepeda, H., Stix, J., 1997. 'Tornillo'-type seismic signals at Galeras volcano, Colombia, 1992–1993. J. Volcanol. Geotherm. Res. 77, 159–171.

Neuberg, J., Luckett, R., Baptie, B., Olsen, K., 2000. Models of tremor and low-frequency earthquake swarms on Montserrat. J. Volcanol. Geotherm. Res. 101, 83–114.

Ohminato, T., Chouet, B.A., Dawson, Ph., Kedar, Sh., 1998. Waveform inversion of very long period impulsive signals associated wiht magmatic injection beneath Kilauea Volcano, Hawaii. J. Geophys. Res. 103, 23839–23862.

Ortiz, R., García, A., Aparicio, A., Blanco, I., Felpeto, A., del Rey, R., Villegas, M., Ibáñez, J.M., Morales, J., Del Pezzo, E., Olmedillas, J.C., Astiz, M., Vila, J., Ramos, M., Viramonte, J.G., Risso, C., Caselli, A., 1997. Monitoring of the volcanic activity of Deception Island, South Shetland Islands, Antarctica (1986–1995). In: The Antarctic Region: Geological Evolution and Processes, pp. 1071–1076.

Pelayo, A.M., Wiens, D.A., 1989. Seismotectonics and relative plate motions in the Scotia Sea region. J. Geophys. Res. 94, 7293–7320.

Ramos, E.G., Hamburger, M.W., Pavlis, G.L., Laguerta, E.P., 1999. The low-frequency earthquake swarms at Mount Pinatubo, Philippines: Implications for magma dynamics. J. Volcanol. Geotherm. Res. 92, 295–320.

Saccorotti, G., Almendros, J., Carmona, E., Ibáñez, J.M., Del Pezzo, E., 2001. Slowness anomalies from two dense seismic arrays at Deception Island, Antarctica. Bull. Seismol. Soc. Am. 91, 561–571.

Saccorotti, G., Carmona, E., Ibáñez, J.M., Del Pezzo, E., 2002. Spatial characterization of the Agron, southern Spain, 1988–1989 seismic series. Phys. Earth Planet. Inter. 129, 13–29.